



Flares, Rotation, and Planets of the AU Mic System from TESS Observations

Emily A. Gilbert^{1,2,3,4,5} , Thomas Barclay^{2,4} , Elisa V. Quintana⁴ , Lucianne M. Walkowicz³ , Laura D. Vega^{4,6} , Joshua E. Schlieder⁴ , Teresa Monsue⁴ , Bryson L. Cale⁷ , Kevin I. Collins⁷ , Eric Gaidos⁸ , Mohammed El Mufti⁷ , Michael A. Reefe⁷ , Peter Plavchan⁷ , Angelle Tanner⁹, Robert A. Wittenmyer¹⁰ , Justin M. Wittrock⁷ , Jon M. Jenkins¹¹ , David W. Latham¹² , George R. Ricker¹³ , Mark E. Rose¹¹ , S. Seager^{13,14,15} , Roland K. Vanderspek¹³ , and Joshua N. Winn¹⁶

¹ Department of Astronomy and Astrophysics, University of Chicago, 5640 S. Ellis Avenue, Chicago, IL 60637, USA; emilygilbert@uchicago.edu

² University of Maryland, Baltimore County, 1000 Hilltop Circle, Baltimore, MD 21250, USA

³ The Adler Planetarium, 1300 South Lakeshore Drive, Chicago, IL 60605, USA

⁴ NASA Goddard Space Flight Center, 8800 Greenbelt Road, Greenbelt, MD 20771, USA

⁵ GSFC Sellers Exoplanet Environments Collaboration, USA

⁶ Vanderbilt University, Department of Physics & Astronomy, 6301 Stevenson Center Lane, Nashville, TN 37235, USA

⁷ Department of Physics and Astronomy, George Mason University, Fairfax, VA, USA

⁸ Department of Earth Sciences, University of Hawai'i at Manoa, Honolulu, HI 96822 USA

⁹ Mississippi State University, Department of Physics & Astronomy, Hilburn Hall, Starkville, MS 39762, USA

¹⁰ University of Southern Queensland, Centre for Astrophysics, West Street, Toowoomba, QLD 435 Australia

¹¹ NASA Ames Research Center, Moffett Field, CA, 94035, USA

¹² Center for Astrophysics | Harvard & Smithsonian, 60 Garden Street, Cambridge, MA 02138, USA

¹³ Department of Physics and Kavli Institute for Astrophysics and Space Research, Massachusetts Institute of Technology, Cambridge, MA 02139, USA

¹⁴ Department of Earth, Atmospheric and Planetary Sciences, Massachusetts Institute of Technology, Cambridge, MA 02139, USA

¹⁵ Department of Aeronautics and Astronautics, MIT, 77 Massachusetts Avenue, Cambridge, MA 02139, USA

¹⁶ Department of Astrophysical Sciences, Princeton University, 4 Ivy Lane, Princeton, NJ 08544, USA

Received 2021 April 21; revised 2021 August 30; accepted 2021 September 2; published 2022 March 3

Abstract

AU Mic is a young (~ 24 Myr), pre-main-sequence M dwarf star that was observed in the first month of science observations of the Transiting Exoplanet Survey Satellite (TESS) and reobserved 2 years later. This target has photometric variability from a variety of sources that is readily apparent in the TESS light curves; spots induce modulation in the light curve, flares are present throughout (manifesting as sharp rises with slow exponential decay phases), and transits of AU Mic b may be seen by eye as dips in the light curve. We present a combined analysis of both TESS Sector 1 and Sector 27 AU Mic light curves including the new 20 s cadence data from TESS Year 3. We compare flare rates between both observations and analyze the spot evolution, showing that the activity levels increase slightly from Sector 1 to Sector 27. Furthermore, the 20 s data collection allows us to detect more flares, smaller flares, and better resolve flare morphology in white light as compared to the 2 minute data collection mode. We also refine the parameters for AU Mic b by fitting three additional transits of AU Mic b from Sector 27 using a model that includes stellar activity. We show that the transits exhibit clear transit timing variations with an amplitude of ~ 80 s. We also detect three transits of a $2.8 R_{\oplus}$ planet, AU Mic c, which has a period of 18.86 days.

Unified Astronomy Thesaurus concepts: [Exoplanet detection methods \(489\)](#); [Red dwarf flare stars \(1367\)](#); [Transit timing variation method \(1710\)](#); [Astronomy data modeling \(1859\)](#); [M dwarf stars \(982\)](#)

1. Introduction

AU Mic (TIC 441420236, GJ 803) is a young (24 ± 3 Myr; Bell et al. 2015), nearby (9.9 ± 0.1 pc; Gaia Collaboration et al. 2018), bright ($K = 4.5$ mag; Stauffer et al. 2010) M1 pre-main-sequence star. AU Mic is known for its frequent white light flares and its debris disk (Kalas et al. 2004) that contains moving large-scale features (Boccaletti et al. 2015, 2018). The recent detection of a planet, AU Mic b, (Plavchan et al. 2020) and a candidate planet c (Martoli et al. 2021) orbiting the star make this target even more intriguing. This pre-main-sequence star provides us with valuable insight into how planetary systems are formed and develop and evolve in stellar infancy. For these reasons, AU Mic is an extremely well-studied star, and has been for decades.

AU Mic has been theorized to be a young star (Eggen 1968; Kunkel 1970; Wilson & Woolley 1970) and known to have flares since the late 1960s/early 1970s¹⁷ (Kunkel 1970, 1973). Its high amplitude photometric variability was first identified by Torres et al. (1972) who observed the star 50 times over a 3 month duration and suggested that dark surface spots were the cause of a 4.865 day modulation with a peak-to-peak amplitude of approximately 30%. This photometric variability showed significant changes in amplitude during observations taken in the 1970 s and 1980 s (Butler et al. 1987), with the spot modulation similar to what we now see with two distinct spots or spot groups, apparently appearing in 1981 (Rodono et al. 1986).

The youth of AU Mic was verified via its membership in the β Pictoris Moving Group (Zuckerman et al. 2001; Gagné et al. 2018). The star was first identified as having common galactic kinematics and a similar age to the eponymous β Pictoris by

¹⁷ AU Mic is listed by catalog number 395 in Eggen (1968) who suggested that it was one of two that “could represent stars that are still in the pre-main-sequence stage of their evolution”.

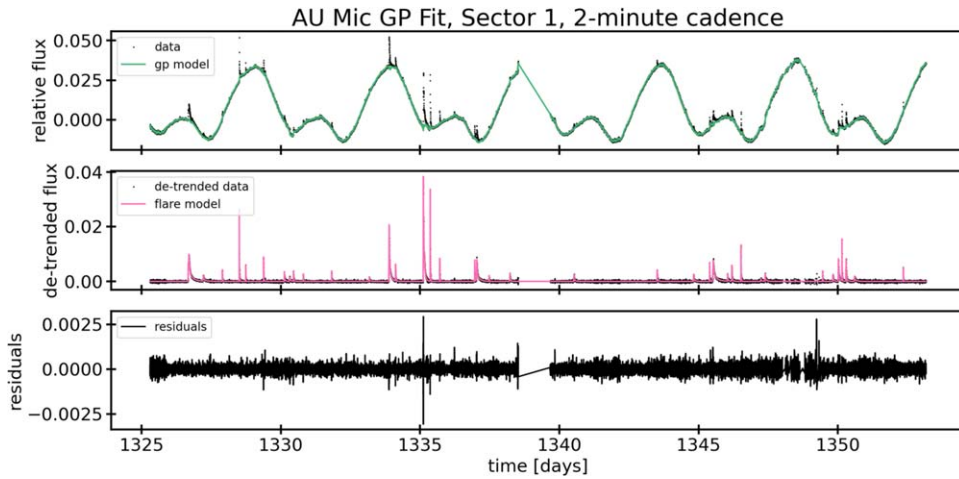


Figure 1. TESS Sector 1, 2 minute cadence observations of AU Mic. The top panel shows our GP spot model, the middle shows our flare model, and the bottom shows the residuals.

Barrado y Navascués et al. (1999). Subsequent study over the last two decades has firmly placed the star in the young stellar association and led to detailed estimates of its age using multiple methods. Consistent age estimates in the range of approximately 20–30 Myr have been found for the group (and thereby AU Mic) using isochronal analyses (Mamajek & Bell 2014; Bell et al. 2015), lithium depletion boundary studies (Binks & Jeffries 2014; Malo et al. 2014; Macintosh et al. 2015; Shkolnik et al. 2017), and dynamical mass measurements as well as evolution model analyses of known binaries (Nielsen et al. 2016; Montet et al. 2015). Here, we adopt the 24 ± 3 Myr isochronal age from Bell et al. (2015) for AU Mic. Recent summaries describing the history of the β Pic group are available in Brandt et al. (2014) and Nielsen et al. (2016).

AU Mic continues to be studied and monitored by a wide variety of instruments to this day, including ongoing observation by the Transiting Exoplanet Survey Satellite (TESS). TESS is an all-sky mission designed to search for planets transiting nearby stars (Ricker et al. 2015) using short-cadence, high-precision photometry. TESS started regular science operation on 2018 July 25, when it began observing in the Southern Ecliptic Hemisphere. TESS observed the Southern Ecliptic sky in 13 sectors, each ~ 28 days long, totaling 1 year of observations. During this time, TESS observed a number of stars at 2 minute cadence and collected full frame images (FFIs) every 30 minutes. After a year of observing in the south, TESS observed the Northern Ecliptic Hemisphere, in a similar pattern of 13 sectors at 2 and 30 minute cadences. TESS completed its primary mission in 2020 July. Now in its extended mission, TESS once again observed in the Southern Ecliptic Hemisphere. TESS observed in a similar pattern to its first year of observations, observing the initial 13 sectors in order. In the extended mission, the data products have improved time sampling. For each sector there are >500 20 s cadence targets; small cutouts called postage stamps are available at a 2 minute cadence for 20,000 targets per sector, and FFI exposures are now captured every 10 minutes.

AU Mic b was discovered using observations from the first sector of TESS observations taken in 2018 July (Plavchan et al. 2020). The AU Mic light curve also showed significant variation as a result of stellar activity. Now, TESS has completed its third year of operations. AU Mic was reobserved in Sector 27 at 20 s cadence. This 2 year gap in observations

plus the new higher cadence data make this system worthy of a reevaluation in order to refine the parameters for planet b and further characterize the activity of the host star.

Herein, we present an overview of the data acquisition for both TESS observations (Section 2). We then analyze the white light flares present in both the Sector 1 and Sector 27 TESS light curves and compare the results using both 2 minute and 20 s cadence data (Section 3). Next, we analyze the rotational spot modulation seen in both light curves (Section 4). We then present revised parameters for AU Mic b by fitting all five transits seen by TESS (Section 5). Finally, we conclude by fitting three transits of AU Mic c, a tentative detection of which was initially presented in Plavchan et al. (2020; Section 6).

2. Data and Observations

TESS observed AU Mic twice: once in the first month of science operation (2018 July) and once in the third year of science operation (2020 July). The first observation of AU Mic¹⁸ occurred during TESS Sector 1 observations using Camera 1, CCD 4. These observations were taken at 2 minute cadence and were completed during orbits 9 and 10 over the course of 27.9 days, with a 1.13 day interruption for data downlink between orbits, see Figure 1. Observations started on 2018 July 25 at 19:00:27 UTC and ended on 2018 August 22 at 16:14:51 UTC (TESS Julian Date (TJD)¹⁹ 1325.29278 to 1353.17778).

During the period of time from 2018 August 16 16:00 UTC to 2018 August 18 16:00 UTC (TJD 13471349), TESS had an improperly configured fine pointing mode calibration, contributing excess jitter and resulting in a significant noise increase. We filter out this data using data quality flags, resulting in some gaps in observation.

AU Mic was observed again²⁰ in TESS Sector 27 (TESS orbits 61 and 62), for 23.35 days of science operations (see

¹⁸ AU Mic was included on the 2 minute cadence list thanks to its inclusion on the following TESS Cycle 1 Guest Investigator (GI) programs: G011264/PI Davenport; G011175/PI Mann; G011180/PI Dressing; G011185/PI Davenport; G011266/PI Schlieder; G011176/PI Czekala; and G011239/PI Kowalski.

¹⁹ TESS timestamps are Barycentric Julian Date—2457000.

²⁰ AU Mic was a target in 10 Cycle 3 GI proposals: G03263/PI Plavchan; G03273/PI Vega; G03141/PI Newton; G03063/PI Llana; G03205/PI Monsue; G03272/PI Burt; G03227/PI Davenport; G03228/PI Million; G03226/PI Silverstein; G03202/PI Paudel.

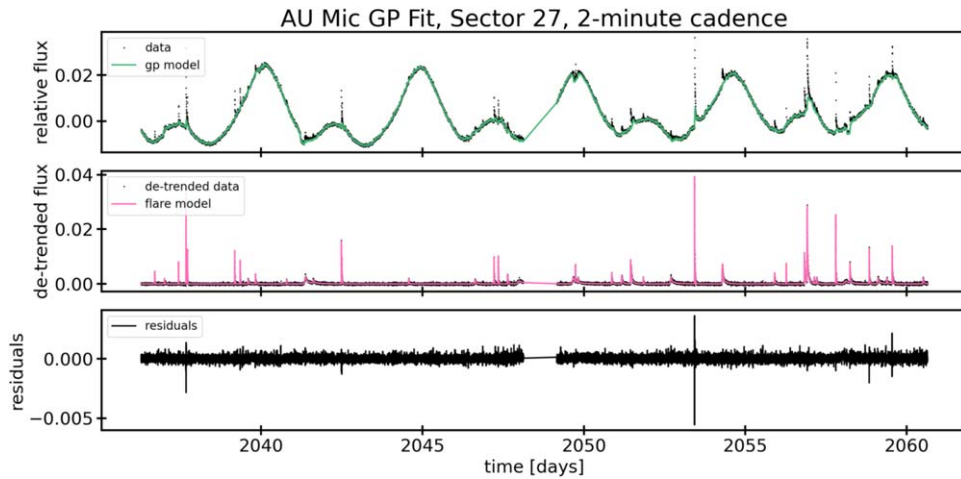


Figure 2. TESS Sector 27, 2 minute cadence observations of AU Mic. The top panel shows our GP spot model, the middle shows our flare model, and the bottom shows the residuals.

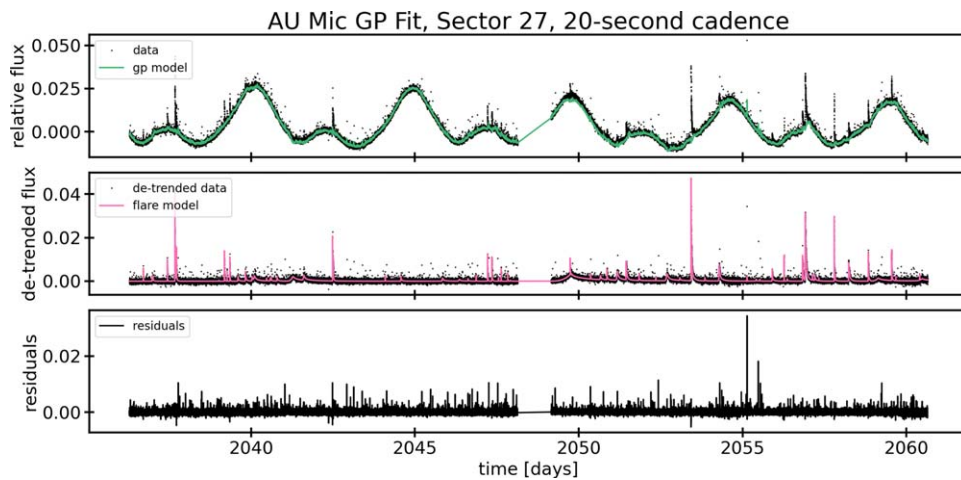


Figure 3. TESS Sector 27, 20 s cadence observations of AU Mic. The top panel shows our GP spot model, the middle shows our flare model, and the bottom shows the residuals.

Figures 2 and 3). The observations began on 2020 July 5 at 18:31:16 UTC and ended on 2020 July 30 at 03:21:15 UTC (TJD 2036.27320 through 2060.64125). A 1.02 day gap for data downlink began on 2020 July 17 15:01:15 UTC. These data were collected at both 20 s and at 2 minute cadence. The 20 s cadence postage stamps consist of 10 coadds of 1.98 s exposures.

We used the `lightkurve` (Lightkurve Collaboration et al. 2018) package to download the AU Mic TESS light curves for Sectors 1 and 27 from the Mikulski Archive for Space Telescopes (MAST archive). The Science Processing Operations Center (SPOC) processing the 2 minute and 20 second data to calibrate the image data, extract simple aperture photometry, and identify and remove systematic effects from the resulting light curves (Jenkins et al. 2016). We chose to use the Presearch Data Conditioning (PDC_SAP) light curves in our analysis (Stumpe et al. 2012, 2014; Smith et al. 2012), which have been corrected for instrumental effects and for crowding. We used the “hardest” bitmask filter in `lightkurve`, and further filtered the data by removing NaNs. We confirmed by comparing these light curves to the unmasked light curves that no flares were removed in this process. This left us with light curves with 25.07, 23.29, and 22.57 days

worth of observations for Sector 1; Sector 27, 2 minute; and Sector 27, 20 s data, respectively.

3. Analysis of White Light Flares

We started by using an iterative Savitzky–Golay filter in order to flatten out the spot modulation in the raw light curves in preparation for flare detection. For the 2 minute cadence data, we iterated three times with a 10 hour window and fit a fourth-order polynomial. With the 20 s cadence data, we iterated over five Savitzky–Golay fits, with a window length of five hours with a third-order polynomial. Then we detected flares using a modified version of the `bayesflare` Python package (Pitkin et al. 2014) that we have adapted to run on TESS short-cadence data (both 2 minute and 20 s cadences). `bayesflare` uses Bayesian inference to detect flares in the data by running a sliding window over the data, comparing the data to the template, and ascribing an odds ratio to each data point. We used a flare template that models flares as a Gaussian rise ranging from 0 to 1.5 hr in duration followed by an exponential decay term ranging from half an hour to 3 hr in duration (modified slightly from Pitkin et al. 2014) in order to optimize this software to detect small flares. This method of template matching allows us to differentiate between flares and

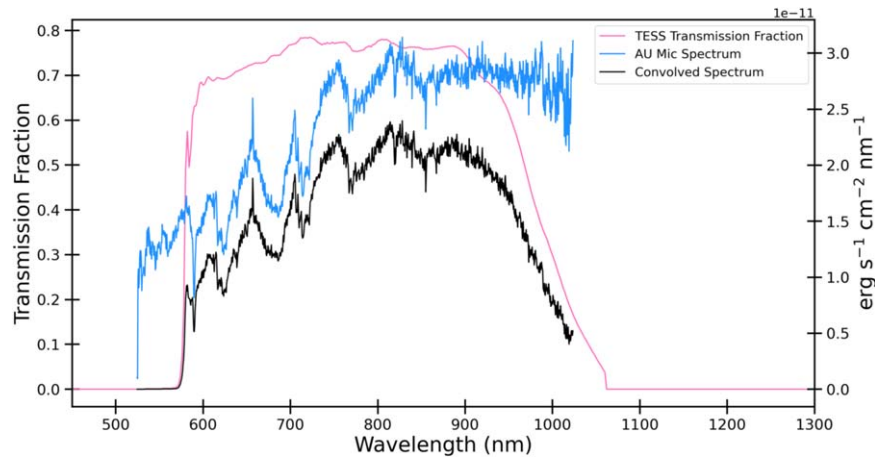


Figure 4. We determine the reference energy for AU Mic by multiplying its spectrum by the TESS transmission function. The resulting convolved spectrum is shown in black. Integrating under the convolved spectrum gives us the quiescent energy emitted by AU Mic within the TESS bandpass.

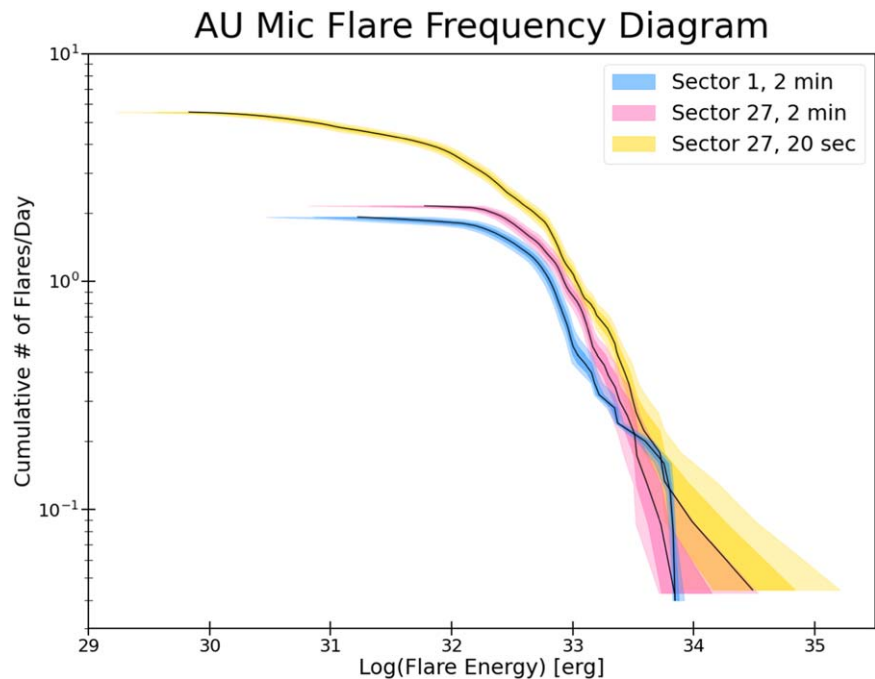


Figure 5. The flare frequency distributions for AU Mic show the flares modeled in both Sectors 1 and 27, as well as 2 minute and 20 s data for Sector 27 with the shaded regions showing the 1σ and 2σ uncertainties. 20 s data significantly improves our ability to detect smaller (on order $\sim 10^{32}$ erg) flares and resolve the full morphology of larger flares, resulting in larger flare energies. 2 minute data represents a lower limit on flare frequency and total energy.

instrumental noise and to accurately detect small flares. We then used `scipy`’s “`find_peaks`” function in order to identify individual peaks within single complex flaring events using a 3σ threshold.

Once flares are detected, `bayesflare` then returns a set of flare parameters: the peak time(s) of each flare, the flare amplitudes, and the durations of each flare. We then used these parameters as initial guesses in a probabilistic model of the flares, with the flare shape based on the Davenport et al. (2014) flare profile. We returned to the original light curve in order to fit the spots and flares simultaneously. This combined fit requires a model implemented by the Theano Development Team (2016) to enable fast automatic differentiation of the function. Toward that end, we have written a small package called `xoflars` that can be used with `PyMC3` (Salvatier et al. 2016) to model flares using the fast-rise, exponential decay

profile of Davenport et al. (2014). In order to fully model the light curve, we include a Gaussian process (GP) component in the model simultaneously with the flare model (Foreman-Mackey et al. 2017; Foreman-Mackey 2018). The GP kernel contains a jitter term describing excess white noise and a periodic term to capture spot modulation in the light curve. The best-fitting models and the residual model can be seen in Figures 1, 2, and 3.

After constructing our model, we sampled over the posterior. Due to the large number of parameters we are fitting, we elected to use `PyMC3`’s Automatic Differentiation Variational Inference algorithm (ADVI; Kucukelbir et al. 2016) to approximate the posterior distribution of our model. We map the posterior distribution with 100,000 iterations. We then draw 3000 samples from the posterior distribution to complete our fit.

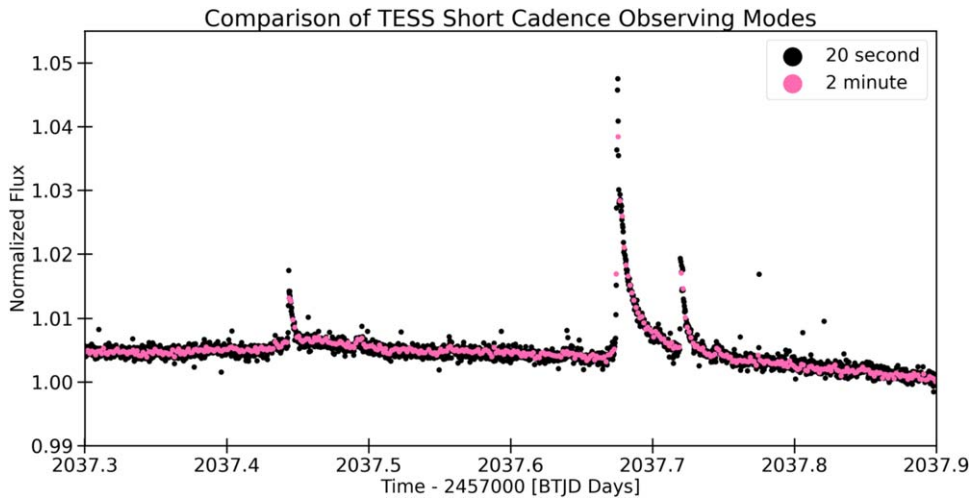


Figure 6. 20 s cadence data (black) allow us to better resolve flare peak amplitudes as compared to the 2 minute cadence data (pink).

From these samples, we were able to determine the distribution of model parameters (and therefore, energies) for each flare. To measure flare energies, we multiplied a flux-calibrated spectrum of AU Mic (Lomax et al. 2018, J. Lomax 2019, private communication; HST program GO-12512) by the TESS response function (Vanderspek et al. 2018) and integrated the result across the TESS wavelength range, see Figure 4. With this result, we found the energy per second per square centimeter emitted by a quiescent AU Mic detected by TESS to be $F_{\text{ref}} = 1.0577 \times 10^{-8} \text{ erg s}^{-1} \text{ cm}^{-2}$, which we subsequently used as a reference flux for the flares. Given the spectrum does not cover the full wavelength range of the TESS bandpass, energies are slightly underestimated.

Integrating under the curve of the flare model yields the equivalent duration of each flare. We were then able to determine the energy (within the TESS bandpass) emitted within each flare by scaling the equivalent duration by the reference energy and distance to AU Mic as follows:

$$E_{\text{abs}} = \int_{t_0}^{t_1} A(t) dt * F_{\text{ref}} * 4\pi d^2, \quad (1)$$

where the distance, obtained by GAIA DR2 parallax (Gaia Collaboration et al. 2018), is given by $d = 9.7248 \pm 0.004 \text{ pc}$, and A is the fractional amplitude of the flare relative to the star’s quiescent flux as determined by our model. We integrated over all 3000 samples for each flare, which allowed us to determine uncertainties for each of the flare energies as shown in the flare frequency distribution presented in Figure 5.

In order to objectively compare the activity levels from Sector 1 to Sector 27, we first investigated flare properties in 2 minute data for both sectors. We removed intervals of instrumental performance issues and calculated flare rates based on the length of time in the remaining data. In 25.07 days of observations from Sector 1, we detected 48 flares (1.855 flares/day), and in 23.29 days of observations in Sector 27, we detected 50 flares (2.147 flares/day). Sector 27 contains more low energy flares than Sector 1, see Figure 5.

We then looked at a comparison between the Sector 27 data obtained at both 2 minute and 20 s cadences. In the 22.57 days of 20 s data used, we detected 125 unique flares (5.54 flares/day). The 20 s data allows us to detect smaller flares than possible with the 2 minute data as shown clearly in Figure 5.

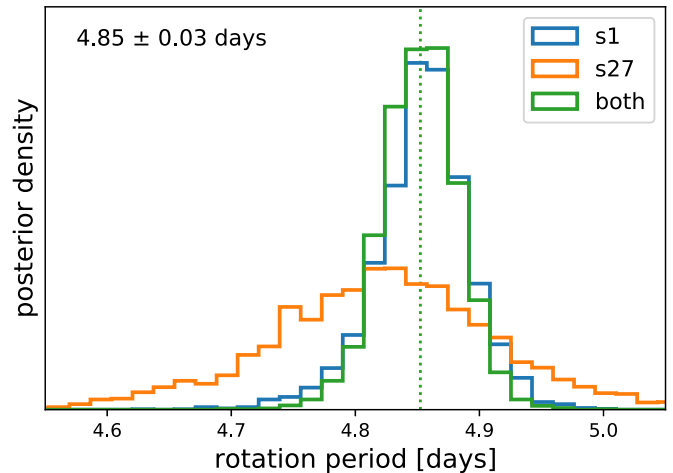


Figure 7. Posterior model of the rotation of AU Mic, measured from the TESS photometric data. The Sector 1 data give stronger constraints on the rotation period, primarily because there seems to be a little more light-curve morphology change or phase drift in the Sector 27 data.

The 20 s data collection also enables us to fully resolve flare morphology, which may occur on timescales that are much faster than 2 minute data collection is capable of capturing, see Figure 6. When we are unable to resolve the peak amplitude of the flare, the flare energies may be underestimated, as evidenced by the discrepancy in energies between the Sector 27 2 minute and 20 s data shown in Figure 5.

4. Spot Evolution

AU Mic has a distinct rotation pattern caused by the spots on the star seen in both sectors of TESS observations, see Figures 1, 2, and 3. The spot pattern of AU Mic appears largely unchanged over the 2 years between TESS observations showing about 4% peak-to-peak variability due to spots in both Sectors 1 and 27, although the amplitude decreased to approximately 3% over the course of Sector 27. Given this persistent morphology, we expect that the same spots or spot groups are likely present during both TESS observations. The consistency in the spot pattern over 2 years shows that AU Mic has long-lived spot patterns. There does not appear to be any significant migration to differentially rotating latitudes on the

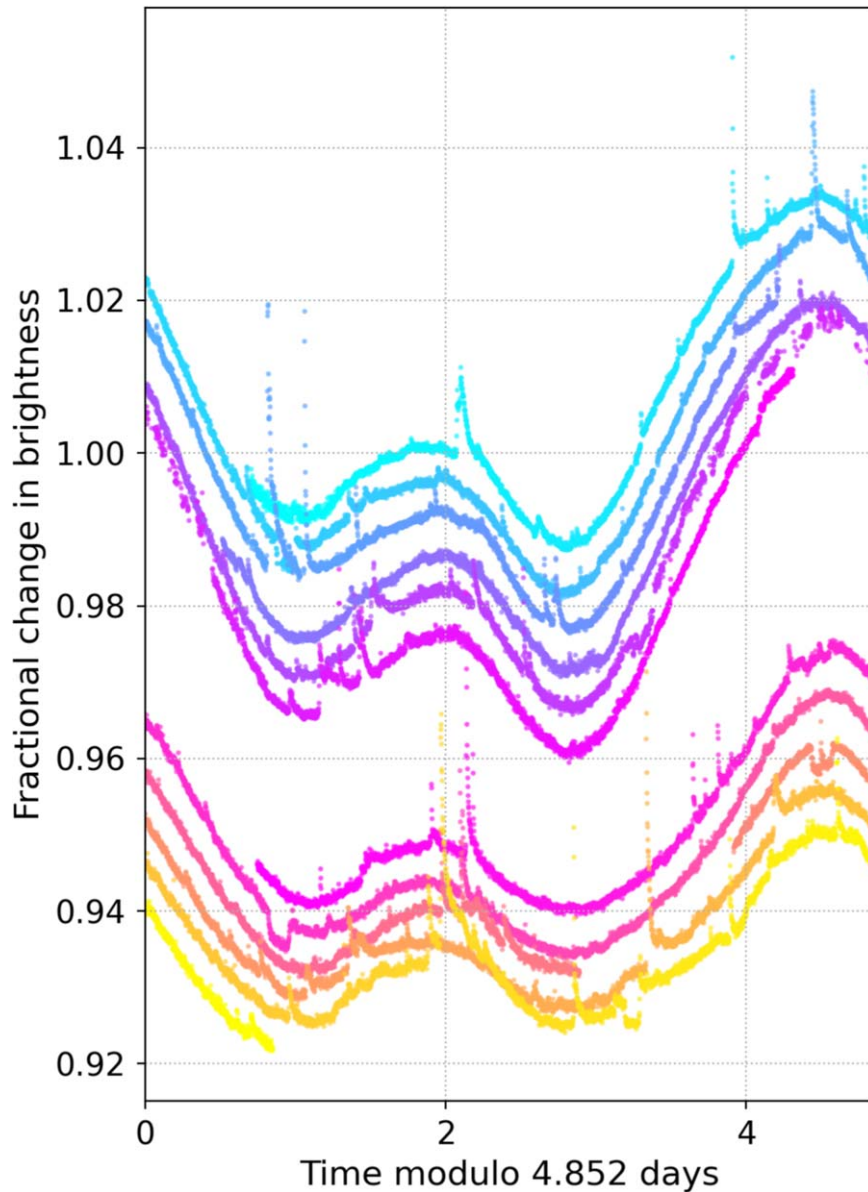


Figure 8. Sector 1 and Sector 27 phase folded at the rotation period of the star, $P = 4.85$ days. Each phase is offset vertically for clarity, with time progressing downward. The overall shape of the light curve shows remarkable consistency over the 2 year observation baseline. The Sector 27 data has been shifted in phase to align with Sector 1 data.

star; though, we are not especially sensitive to phase changes in the light curve as a result of our uncertainty in the rotation period, so we cannot definitively rule changes out. Very long-lived spots have previously been seen on TESS targets, so this is consistent with observations of other M dwarf stars (e.g., Davenport et al. 2020; Robertson et al. 2020).

The significant spot modulation makes it straightforward for us to measure the rotation period of AU Mic. We elected to model these spots on their own using MCMC methods (separate from the variational inference modeling in Section 3) in order to obtain the most robust posteriors for the rotation period. Using the *exoplanet* package (Foreman-Mackey et al. 2021) and *celerite* (Foreman-Mackey et al. 2017; Foreman-Mackey 2018), we modeled the rotation period for each of the two TESS sectors using a periodic Gaussian process kernel. As shown see Figure 7 the period is well constrained. We measure the rotation period, derived from all data sets, to be $P = 4.85 \pm 0.03$ days; we also get consistent

periods when looking at each sector individually. The rotation period is less well constrained in Sector 27 than Sector 1, which we attribute to changes in the morphology of the light curve over rotation cycles in Sector 27 data. This may be due to spot migration and differential rotation on the surface of the star, or could be indicative of evolution in the spot pattern. In Figure 8 we show the two light curves folded on the derived rotation period. While there are changes, the morphology over the 2 years of data changes very little.

As discussed in Section 1, historical observations show this same rotation period dating back 50 yr. Torres et al. (1972) saw a $\sim 30\%$ variability due to spots in *V* band with a 4.865 day rotation period as observed from 1971 July to September. Rodono et al. (1986) showed a series of light curves monitoring AU Mic in several different bands intermittently between 1971 and 1981. These light curves show variations in amplitude, morphology, and phase over time. The amplitudes have varied from $<1\%$ to 30% and therefore the 4% we see today is not

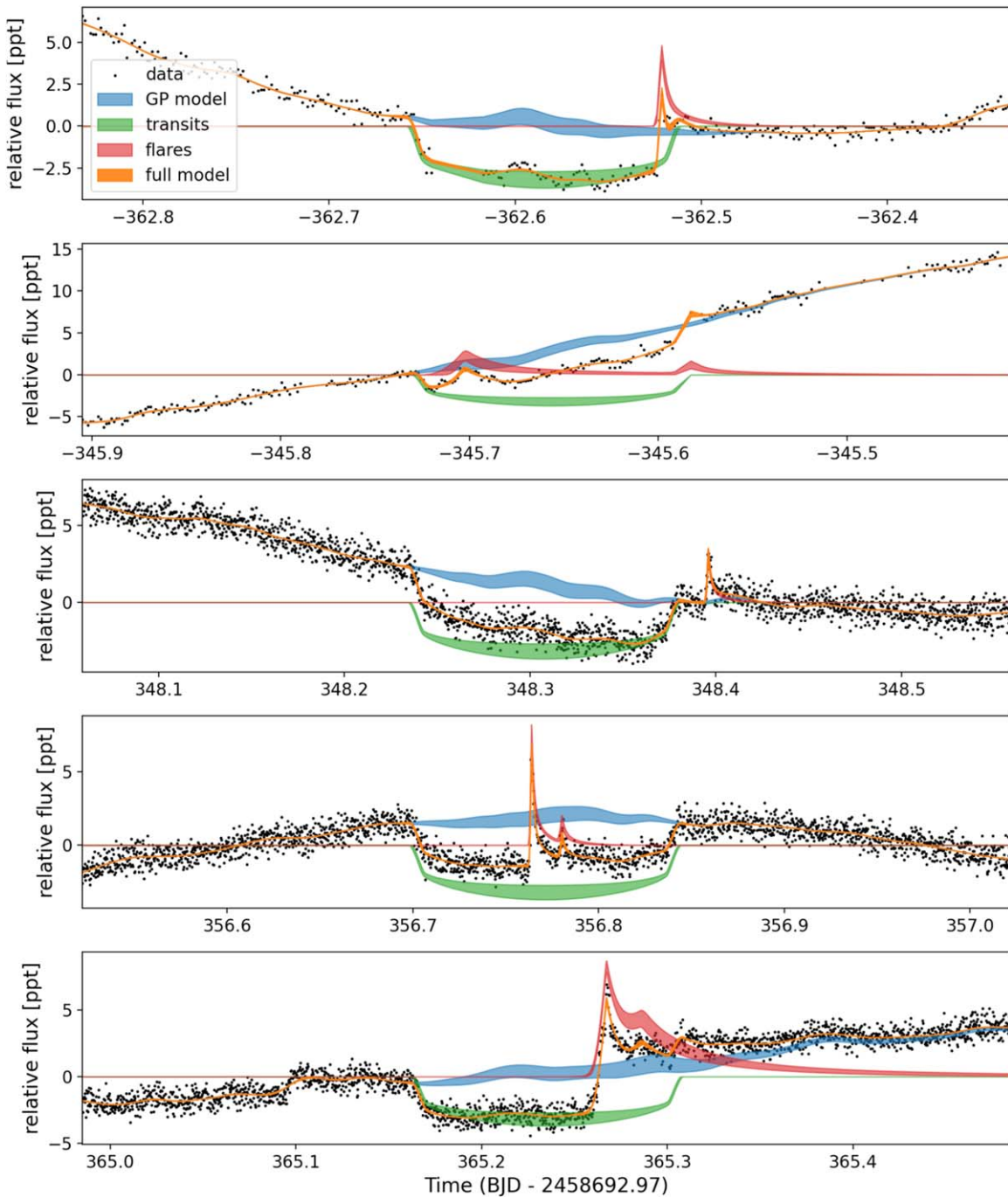


Figure 9. Our model of the five TESS transits of AU Mic b and stellar flares that occur in and around the transit. The first two transits are Sector 1, 2 minute cadence, and the others are Sector 27, 20 s cadence.

unusual. The double-peaked nature has not been observed continuously, but reports since the late 1980s all have the double-peaked structure.

5. Refined Parameters for AU Mic b and Evidence for an Additional Massive Body in the System

Five transits of AU Mic b were observed by TESS. These data are particularly complicated to model because of the stellar variability from spots and flares, which obscure transits and make fits less precise. Our goal in this section is to derive more precise parameters for the planet and to search for any transit timing variations (TTVs) in the TESS transits.

To model the transits, we build upon the work presented in Plavchan et al. (2020) that uses a transit model plus a Gaussian process (GP) to model correlated noise in the light curve using the `exoplanet` package (Foreman-Mackey et al. 2021) and dependencies, primarily `STARRY` (Luger et al. 2019) and `celerite2` (Foreman-Mackey et al. 2017; Foreman-Mackey 2018).

The three additional TESS transits of AU Mic b, observed at 20 s cadence, are significant enhancements in the quantity of data we have available to characterize the planet. However, four out of the five total transits of AU Mic b observed by TESS have flares that occur during or immediately following

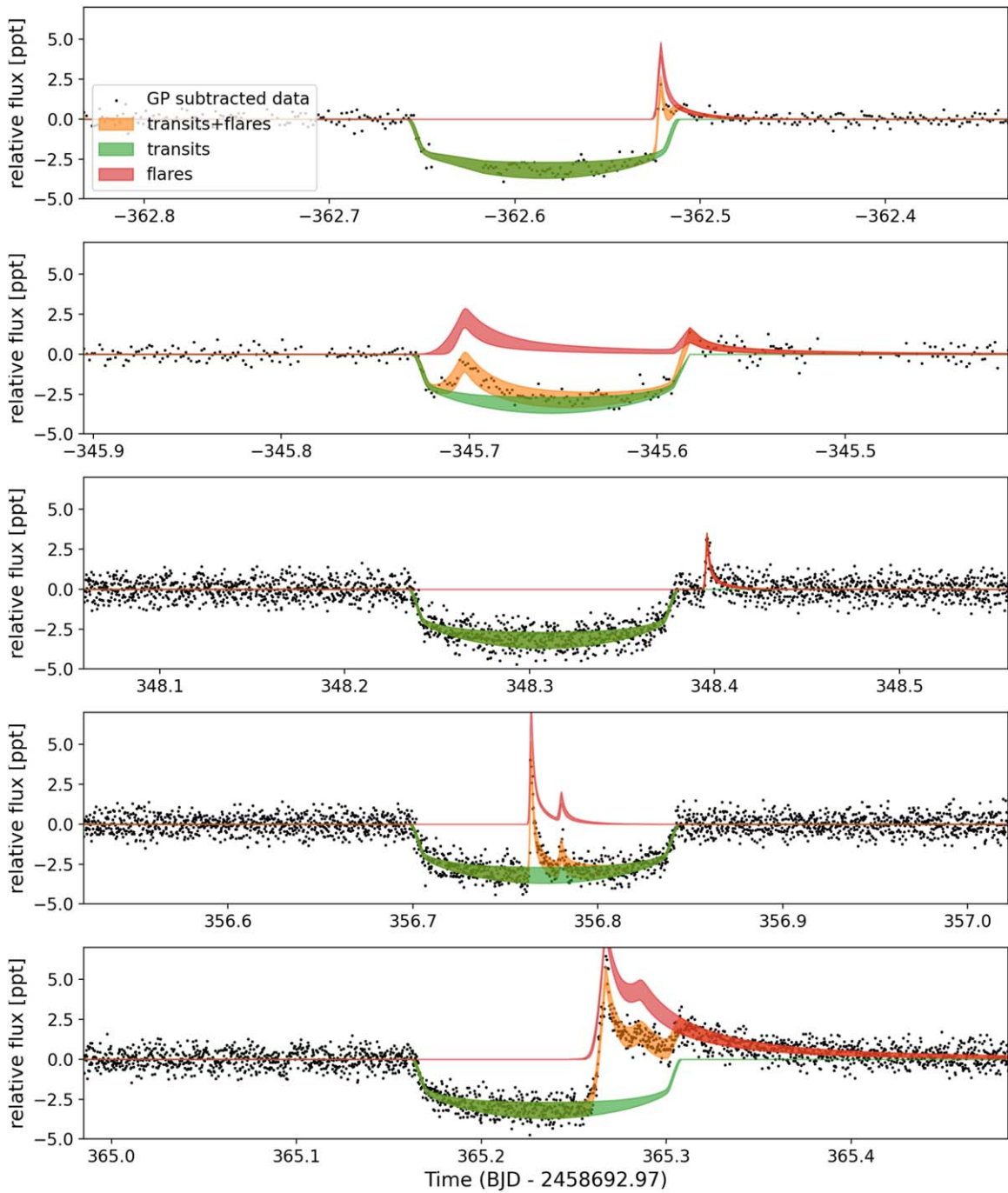


Figure 10. The five TESS transits of AU Mic b with the the best-fitting GP mean model subtracted from the data. The first two transits are Sector 1, 2 minute cadence, and the others are Sector 27, 20 s cadence.

the transit. Because the short-term brightening during flares alters the shape of the transit, how flares are handled during transit fits affects the resulting planet parameters. The final transit observed has a particularly large flaring event that occurs during the final third of the transit and if not modeled correctly, gives the impression that the transit is significantly shorter than expected. In contrast to previous work by Plavchan et al. (2020), who cut out the flares, we instead include them in our model with the goal of more precisely measuring the planet parameters and transit times. We identified times that showed a flare-like shape using the `bayesflare` model, and recorded the approximate peak time, amplitude, and duration. We then

included in the light-curve model a fast-rise exponential-decay component for each flare, following the flare profile described by Davenport et al. (2014). Sampling of the model was performed using the No U-turn Sampler (NUTS; Hoffman & Gelman 2014) implemented in the `PyMC3` framework (Salvatier et al. 2016). We used the `xoflares` Python package (described in Section 3) to model flares in and around the transits. In addition to including the flares in the model, we also allowed the time of the transits to vary so that we could get a constraint on potential TTVs.

Since we are only interested in the transits, and including flares made our model computationally expensive, we opted to

Table 1
AU Mic b Model Parameters

Parameter	Value	+1 σ	-1 σ
Stellar density (g/cc)	1.67	0.38	0.34
Stellar radius (R_{\odot})	0.750	0.029	0.030
Orbital period (d)	8.4630004	0.0000058	0.0000060
T0 (BJD)	2458330.39080	0.00058	0.00057
$R_{\text{planet}}/R_{\text{star}}$	0.0512	0.0020	0.0020
Impact parameter (b)	0.26	0.13	0.17
$e\cos\omega$	0.01	0.38	0.36
$e\sin\omega$	-0.05	0.22	0.20
Eccentricity	0.12	0.16	0.08
Angle of periastron (ω , radians)	-0.3	2.4	2.3
u_1 (limb darkening parameter)	0.50	0.28	0.30
u_2 (limb darkening parameter)	0.05	0.33	0.31
Planet radius (R_{\oplus})	4.19	0.24	0.22
a/R_{\star}	18.5	1.3	1.4
a (au)	0.0644	0.0056	0.0054
Inclination (deg)	89.18	0.53	0.45
Transit duration (hours)	3.56	0.60	0.46

Table 2
AU Mic b Parameters from Plavchan et al. (2020)

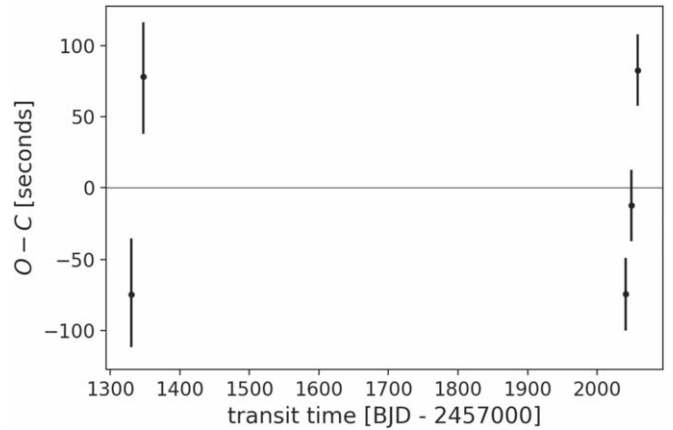
Parameter	Value	+1 σ	-1 σ
Orbital period (d)	8.46321	0.00004	0.00004
T0 (BJD)	2458330.39153	0.00070	0.00068
$R_{\text{planet}}/R_{\text{star}}$	0.00514	0.0013	0.0013
Impact parameter (b)	0.16	0.14	0.11
Eccentricity	0.1	0.17	0.09
Planet radius (R_{\oplus})	4.203	0.202	0.202

Table 3
Times of AU Mic b Transits Observed by TESS

Transit Number	Transit Times (BJD -2457000)
0	1330.38955 \pm 0.00065
2	1347.31733 \pm 0.00066
84	2041.28159 \pm 0.00036
85	2049.74531 \pm 0.00036
86	2058.20941 \pm 0.00037

only include 12 hr of TESS data per transit, centered on the transit. Our model includes parameters for the stellar density, radius, two limb darkening parameters, and a mean value for each 12 hr window. We calculated the stellar density primarily based on Plavchan et al. (2020) values for stellar mass ($0.50 \pm 0.03 M_{\odot}$) and radius ($0.75 \pm 0.03 R_{\odot}$). However, to avoid over-constraining the models in the case of underestimated uncertainties we inflated the uncertainty on the density priors. For stellar density, we used a natural log normal prior with a mean, $\mu = 0.5 \log(\text{g/cc})$, and standard deviation, $\sigma = 0.3$; for radius we used a normal prior with mean, $\mu = 0.75 R_{\odot}$, and standard deviation, $\sigma = 0.03$, bounded at 0.1 and 2; and the limb darkening priors follow the Kipping (2013) formalism for quadratic limb darkening.

We model the stellar variability as a GP representing a stochastically driven, damped harmonic oscillator using

**Figure 11.** Transit times as compared to the derived orbital period for all five transits of AU Mic b observed by TESS.

`celerite2`, parameterized by the oscillation period and standard deviation. The oscillation period and standard deviation are consistent over the different transits. We also include a jitter parameter to describe excess white noise in the data (two jitter parameters in total, one for the 2 minute cadence Sector 1 data, and one for the 20 s cadence Sector 27 data). The planet is parameterized by the planet-to-star radius ratio, impact parameter, orbital eccentricity, and periastron angle (parameterized as $e \sin\omega$ and $e \cos\omega$, and each transit by the transit time from which orbital period and transit epoch are derived). The priors on parameters are mostly weakly constraining lognormal, with orbital eccentricity following Kipping (2013), stellar radius being a normal with parameters from Plavchan et al. (2020), transit times being zero-mean normals with a standard deviation of 30 minutes, and flare peak times being normals with means from the best fit ($t-2458692.97 = -362.52, -345.70, -345.58, 348.40, 356.76, 356.78, 365.27, 365.29$) and a standard deviation of 0.003 days. The time offset in the light curve comes from setting time-zero in the model to be the central time in the whole time series. The planet-to-star radius ratio has a lognormal prior with a mean of 3 and standard deviation of 0.5. Impact parameter is uniformly sampled between 0 and 1 + the planet-to-star radius ratio. Periastron is uniform, but sampled to not see any discontinuities. Jitter and the two GP hyperparameters have inverse gamma priors.

We used the default sampler in `exoplanet`, with four chains, and an initial tuning phase of 5500 samples, followed by 2500 sample draw. The model converged, had Gelman-Rubin diagnostic values (Gelman & Rubin 1992) of <1.001 with a minimum of 2000 independent samples in each model parameter. The model shown in data space is in Figure 9, where the blue curve shows the 80% confidence range of the GP mean model, the green shows the transit and flare model, and the orange shows the sum of these two models. Figure 10 has the GP mean model subtracted, showing the posterior constraints on the transit and flares. We find a best-fitting orbital period of 8.463000 ± 0.000006 days and a planet radius of 4.2 ± 0.2 Earth-radii. We note that this period differs from the period reported by Plavchan et al. (2020) by about 18 s. While small, this difference is highly significant. We attribute the difference to the earlier work not modeling the flares and measuring a transit duration that was slightly too long. The planet parameters are shown in Table 1. We have reproduced the salient parameters derived in Plavchan et al. (2020) for

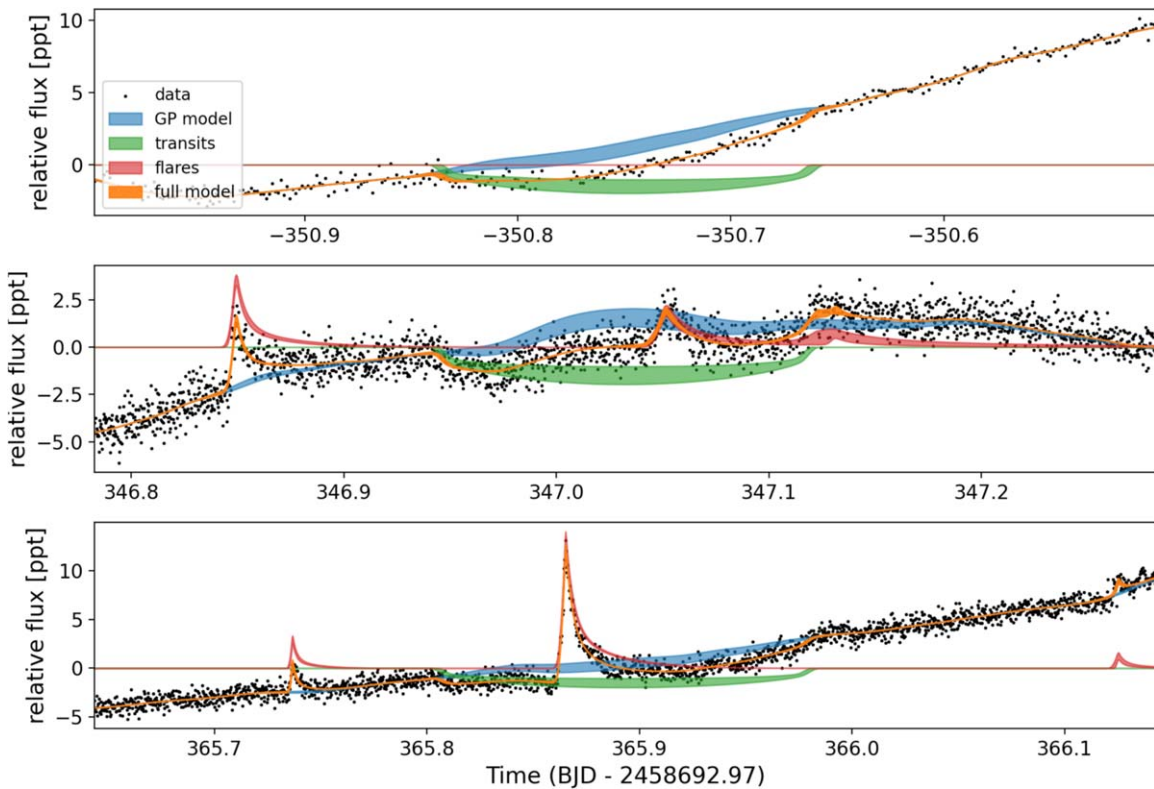


Figure 12. Three transits of AU Mic c. One from Sector 1 observed at 2 minute cadence, and two transits from Sector 27 observed at 20 s cadence.

Table 4
AU Mic c Model Parameters

Parameter	Value	+1 σ	-1 σ
Orbital period (d)	18.858982	0.000053	0.000050
T0 (BJD)	2458342.2239	0.0017	0.0019
$R_{\text{planet}}/R_{\text{star}}$	0.0340	0.0034	0.0033
Impact parameter (b)	0.30	0.21	0.20
$e\cos\omega$	-0.0	0.37	0.37
$e\sin\omega$	-0.05	0.24	0.23
Eccentricity	0.13	0.16	0.09
Angle of periastron (ω , radians)	-0.3	2.5	2.2
Planet radius (R_{\oplus})	2.79	0.31	0.30
a/R_{\star}	31.7	2.6	2.7
a (au)	0.110	0.010	0.010
Inclination (deg)	89.39	0.40	0.38
Transit duration (hours)	4.42	0.92	0.67

comparison in Table 2. Plavchan et al. (2020) used one sector of TESS data coupled with one additional transit observed with Spitzer as compared to two sectors worth of TESS observations used in this work. The stellar density and radius reported in Table 1 are primarily constrained by the prior rather than the data.

The transits are not exactly periodic (see Table 3); this is compelling evidence for TTVs in the TESS data. We find a TTV amplitude of approximately ± 80 s, shown in Figure 11. With such a small TTV amplitude, we were only able to significantly detect the presence of TTVs with the aid of 20 s cadence and precise flare modeling. With only five data points

Table 5
Times of AU Mic c Transits Observed by TESS

Transit Number	Transit Times (BJD - 2457000)
0	1342.2240 ± 0.0018
37	2040.0054 ± 0.0011
38	2058.8663 ± 0.0011

and a 2 year gap between observations, it is difficult to draw too many conclusions from the presence of TTVs, aside from it providing evidence for at least one other massive body in the system, planet c.

6. Detecting AU Mic c

Plavchan et al. (2020) reported the tentative detection of a second planet candidate in the AU Mic system with one potential transit even observed in Sector 1. With the additional data from Sector 27, we see evidence for two additional transits that are not associated with planet b. The duration and depth of the previous event and the two new events are consistent, and the spacing between them implies an orbital period of approximately 18.9 days. We modeled the transits of candidate planet c using the same method described in Section 5, accounting for the transit timing variations shown in Figure 11. The model parameters are provided in Table 4, the transit times are shown in Table 5, and the transit models are shown in Figures 12 and 13.

AU Mic c has a radius of $2.8 \pm 0.30 R_{\oplus}$. Flares occurred during two of the three transits, with a 1.4% amplitude flare occurring close to the center of the final transit. By modeling these flares simultaneously with the data, we can derive an

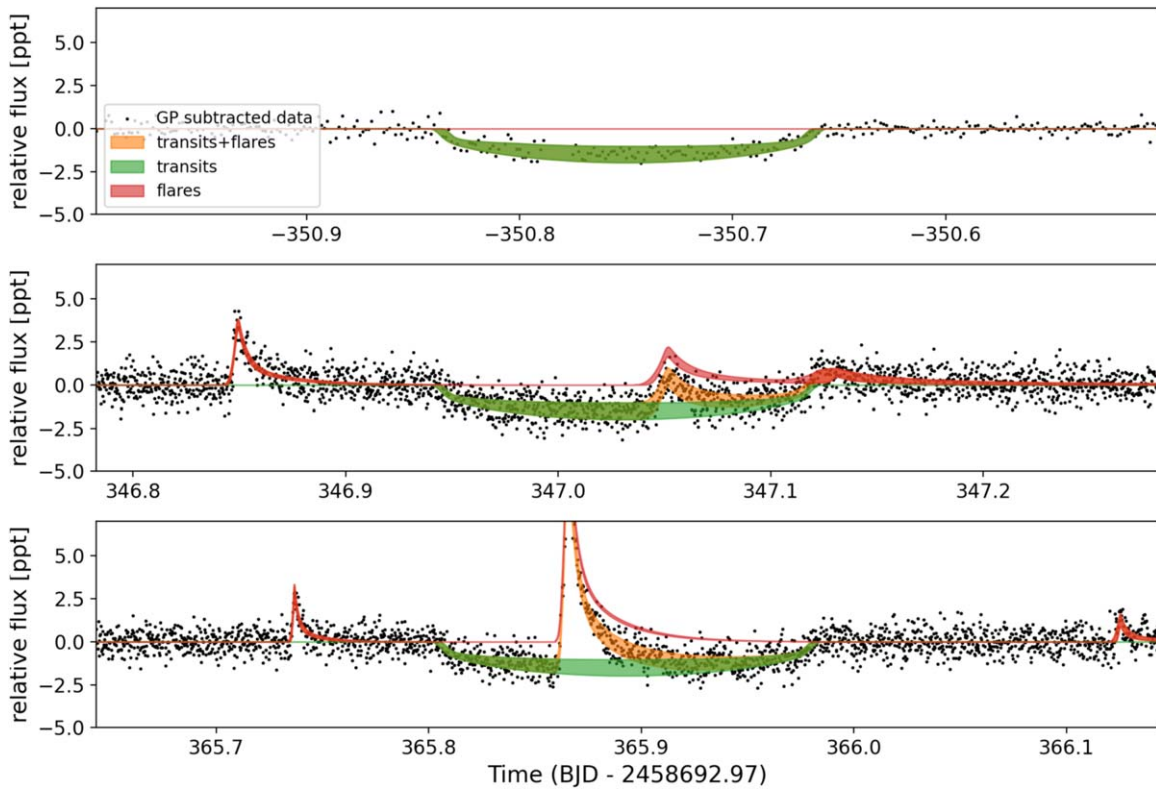


Figure 13. All three transit fits of AU Mic c, with the best-fit GP mean model (stellar rotation and other long-term trends) subtracted off.

accurate radius for the planet. We do note that the radius is fairly uncertain, and this is because the model true transit depth is complicated by the uncertainty in flare amplitudes and durations. For both planets, we detect small, but significant eccentricities. AU Mic c has an orbital period of $2.23\times$ that of AU Mic b, not especially close to any mean motion resonances. Nevertheless, it is possible that AU Mic c is causing the TTVs seen in the AU Mic b transit times (see Section 7). Further observations with Spitzer provide independent confirmation of TTVs, which will be the subject of a subsequent paper (J. M. Wittrock et al. 2022, in preparation).

7. Discussion

AU Mic presents similar, but not identical, levels of activity across the two sectors of TESS observations. The 2 year gap in observations between Sectors 1 and 27 allows us a brief glimpse into the evolution of activity on AU Mic over time. The flare rate increases slightly, but not significantly, from Sector 1 (1.855 flares/day) to Sector 27 (2.147 flares/day) as observed in 2 minute cadence data in each. However, the spot pattern is relatively consistent, with decreasing amplitude in Sector 27 (dropping from 4.3% variability to 3.4%). From our (unresolved) perspective, it is unclear if spots are changing, disappearing, or perhaps appearing more uniformly over the surface of the star, so we are unable to definitively say what may be causing the decrease in amplitude in the variability. Flares, however, are better indicators of the level of activity on a star (Notsu et al. 2013; Doyle et al. 2020; Feinstein et al. 2020). On the Sun, flare rates increase with spot complexity, so the higher flare energies are perhaps indicative of activity cycles occurring on AU Mic similar to those we see on the Sun

where monthly flare rates can vary by a factor of 20 or more (Aschwanden & Freeland 2012).

AU Mic is an extremely well-studied system that many groups have investigated. In particular, Martioli et al. (2021) also looked at the TESS data included in this analysis. Martioli et al. (2021) find planet b to be $4.07 \pm 0.17R_{\oplus}$, consistent with our results. They conduct a similar fit of the potential planet c transits, determining the planet candidate to be $3.24 \pm 0.16R_{\oplus}$ with a period of 18.86 days. While our results agree on the planet period, we find the radius of planet c to be significantly smaller at $2.79 \pm 0.3 R_{\oplus}$ as a result of differing modeling methods. In their analysis, Martioli et al. (2021) find no evidence of transit timing variations, whereas we see evidence for TTVs on the order of ~ 80 s.

We used TTV2fast2furious (Hadden et al. 2018), the derived planet parameters, and planet masses estimated using Forecaster (Chen & Kipping 2017) to infer expected TTV amplitudes driven by interactions between planets b and c. The estimated amplitudes from the software are of order 4 minutes for each planet, which is at the same level of TTV amplitude we measure in the TESS data. While the number of transits we have is fairly limited and therefore a full analysis of TTVs is not appropriate for the data presented here, the observed TTVs would seem to be consistent with interactions between AU Mic b and c.

8. Conclusions

AU Mic was observed twice by TESS: once in Sector 1 at 2 minute cadence and once in Sector 27 at 20 s cadence as well as 2 minute cadence. The introduction of the new 20 s data collection mode coupled with an additional sector of observations with TESS has enabled us to improve transit fits for AU

Mic b and study the activity of AU Mic in unprecedented detail. We detected and modeled flares in all available sectors of data, and show that AU Mic has grown slightly more active over the 2 year baseline from Sector 1 to Sector 27. Furthermore, the 20 s data collection mode allows us to detect more flares at smaller energies as well as resolve white light flare morphologies better than the 2 minute cadence alone. While the white light flare rate increases slightly from Sector 1 to Sector 27, the spot pattern of the star remains largely unchanged, indicating the likely persistence of a particular set of spots at preferred latitudes.

We also used three additional transits of planet b observed by TESS in Sector 27 at 20 s cadence in order to refine the original planet fits as described in Plavchan et al. (2020) and report the detection of TTVs. Due to the frequent white light flares emitted by AU Mic, it was necessary to model both the flares and transits simultaneously in order to derive the most precise fits for the planet, AU Mic b. Furthermore, by allowing the time of the transits to vary in our fits, we determined that the transits do not show a constant linear ephemeris, and have a TTV amplitude of ± 80 s. We also saw two transits not associated with planet b. We fit these in conjunction with the tentative transit described by Plavchan et al. (2020) in Sector 1, and derived parameters for planet c, showing it to be a planet candidate with radius $2.79 \pm 0.30 R_{\oplus}$. These results demonstrate the remarkable value of the 20 s light curves for gaining enhanced insight into both stellar magnetic activity and for obtaining a better understanding of planet parameters and dynamics.

This paper makes use of the 20 s cadence mode introduced in the TESS extended mission. We thank those on the TESS team who made this data collection mode possible.

This paper includes data collected by the TESS mission, which are publicly available from the Mikulski Archive for Space Telescopes (MAST). Funding for the TESS mission is provided by NASA's Science Mission directorate. We acknowledge the use of public TESS Alert data from pipelines at the TESS Science Office and at the TESS Science Processing Operations Center.

This research has made use of the Exoplanet Follow-up Observation Program website, which is operated by the California Institute of Technology, under contract with the National Aeronautics and Space Administration under the Exoplanet Exploration Program.

Resources supporting this work were provided by the NASA High-End Computing (HEC) Program through the NASA Advanced Supercomputing (NAS) Division at Ames Research Center for the production of the SPOC data products.

We are grateful to Jamie Lomax and John Wisniewski who kindly provided us with the HST spectrum used in this work.



E.A.G. thanks the LSSTC Data Science Fellowship Program, which is funded by LSSTC, NSF Cybertraining Grant #1829740, the Brinson Foundation, and the Moore Foundation; her participation in the program has benefited this work. E.A.G. is thankful for support from GSFC Sellers Exoplanet Environments Collaboration (SEEC), which is funded by the NASA Planetary Science Divisions Internal Scientist Funding Model. The material is based upon work supported by NASA under award number 80GSFC21M0002. This work was also supported by NASA awards 80NSSC19K0104 and 80NSSC19K0315.

This work was supported by grants to P.P. and L.V. from NASA (awards 80NSSC20K0251, 80NSSC21K0349, and 80NSSC21K0241), the National Science Foundation (Astronomy and Astrophysics grants 1716202 and 2006517), and the Mount Cuba Astronomical Foundation.

Facility: TESS.

Software: astropy (Astropy Collaboration et al. 2013, 2018), celerite2 (Foreman-Mackey et al. 2017; Foreman-Mackey 2018), exoplanet (Foreman-Mackey et al. 2021), Forecaster (Chen & Kipping 2017), IPython (Perez & Granger 2007), Jupyter (Kluyver et al. 2016), Lightkurve (Lightkurve Collaboration et al. 2018), Matplotlib (Hunter 2007), NumPy (Harris et al. 2020), PyMC3 (Salvatier et al. 2016), STARRY (Luger et al. 2019; Agol et al. 2020), Theano (Theano Development Team., 2016), xoflars (Barclay & Gilbert 2020) TTV2Fast2Furious (Hadden et al. 2018).

ORCID iDs

Emily A. Gilbert  <https://orcid.org/0000-0002-0388-8004>
 Thomas Barclay  <https://orcid.org/0000-0001-7139-2724>
 Elisa V. Quintana  <https://orcid.org/0000-0003-1309-2904>
 Lucianne M. Walkowicz  <https://orcid.org/0000-0003-2918-8687>
 Laura D. Vega  <https://orcid.org/0000-0002-5928-2685>
 Joshua E. Schlieder  <https://orcid.org/0000-0001-5347-7062>
 Teresa Monsue  <https://orcid.org/0000-0003-3896-3059>
 Bryson L. Cale  <https://orcid.org/0000-0002-2078-6536>
 Kevin I. Collins  <https://orcid.org/0000-0003-2781-3207>
 Eric Gaidos  <https://orcid.org/0000-0002-5258-6846>
 Mohammed El Mufti  <https://orcid.org/0000-0001-8364-2903>
 Michael A. Reefe  <https://orcid.org/0000-0003-4701-8497>
 Peter Plavchan  <https://orcid.org/0000-0002-8864-1667>
 Robert A. Wittenmyer  <https://orcid.org/0000-0001-9957-9304>
 Justin M. Wittrock  <https://orcid.org/0000-0002-7424-9891>
 Jon M. Jenkins  <https://orcid.org/0000-0002-4715-9460>
 David W. Latham  <https://orcid.org/0000-0001-9911-7388>
 George R. Ricker  <https://orcid.org/0000-0003-2058-6662>
 Mark E. Rose  <https://orcid.org/0000-0003-4724-745X>
 S. Seager  <https://orcid.org/0000-0002-6892-6948>
 Roland K. Vanderspek  <https://orcid.org/0000-0001-6763-6562>
 Joshua N. Winn  <https://orcid.org/0000-0002-4265-047X>

References

- Agol, E., Luger, R., & Foreman-Mackey, D. 2020, *AJ*, 159, 123
 Aschwanden, M. J., & Freeland, S. L. 2012, *ApJ*, 754, 112
 Astropy Collaboration, Price-Whelan, A. M., Sipőcz, B. M., et al. 2018, *AJ*, 156, 123
 Astropy Collaboration, Robitaille, T. P., Tollerud, E. J., et al. 2013, *A&A*, 558, A33
 Barclay, T., & Gilbert, E. 2020, mrtommyb/xoflars, v0.2.1, Zenodo, doi:10.5281/zenodo.4156285
 Barrado y Navascués, D., Stauffer, J. R., Song, I., & Caillault, J.-P. 1999, *ApJL*, 520, L123
 Bell, C. P. M., Mamajek, E. E., & Naylor, T. 2015, *MNRAS*, 454, 593
 Binks, A. S., & Jeffries, R. D. 2014, *MNRAS*, 438, L11
 Boccaletti, A., Sezestre, E., Lagrange, A.-M., et al. 2018, *A&A*, 614, A52
 Boccaletti, A., Thalmann, C., Lagrange, A.-M., et al. 2015, *Natur*, 526, 230
 Brandt, T. D., Kuzuhara, M., McElwain, M. W., et al. 2014, *ApJ*, 786, 1
 Butler, C. J., Doyle, J. G., Andrews, A. D., et al. 1987, *A&A*, 174, 139
 Chen, J., & Kipping, D. 2017, *ApJ*, 834, 17
 Davenport, J. R. A., Hawley, S. L., Hebb, L., et al. 2014, *ApJ*, 797, 122
 Davenport, J. R. A., Mendoza, G. T., & Hawley, S. L. 2020, *AJ*, 160, 36

- Doyle, L., Ramsay, G., & Doyle, J. G. 2020, *MNRAS*, **494**, 3596
- Eggen, O. J. 1968, *ApJS*, **16**, 49
- Feinstein, A. D., Montet, B. T., Ansdell, M., et al. 2020, *AJ*, **160**, 219
- Foreman-Mackey, D. 2018, *RNAAS*, **2**, 31
- Foreman-Mackey, D., Agol, E., Ambikasaran, S., & Angus, R. 2017, *AJ*, **154**, 220
- Foreman-Mackey, D., Luger, R., Agol, E., et al. 2021, *JOSS*, **6**, 3285
- Gagné, J., Mamajek, E. E., Malo, L., et al. 2018, *ApJ*, **856**, 23
- Gaia Collaboration, Brown, A. G. A., Vallenari, A., et al. 2018, *A&A*, **616**, A1
- Gelman, A., & Rubin, D. B. 1992, *StaSc*, **7**, 457
- Hadden, S., Barclay, T., Payne, M. J., & Holman, M. J. 2018, arXiv:1811.01970
- Harris, C. R., Millman, K. J., van der Walt, S. J., et al. 2020, *Natur*, **585**, 357
- Hoffman, M. D., & Gelman, A. 2014, *J. Mach. Learn. Res.*, **15**, 1593
- Hunter, J. D. 2007, *CSE*, **9**, 90
- Jenkins, J. M., Twicken, J. D., McCauliff, S., et al. 2016, *Proc. SPIE*, **9913**, 99133E
- Kalas, P., Liu, M. C., & Matthews, B. C. 2004, *Sci*, **303**, 1990
- Kipping, D. M. 2013, *MNRAS*, **435**, 2152
- Kluyver, T., Ragan-Kelley, B., Pérez, F., et al. 2016, in *Positioning and Power in Academic Publishing: Players, Agents and Agendas*, ed. F. Loizides & B. Schmidt (Amsterdam: IOS Press), 87
- Kucukelbir, A., Tran, D., Ranganath, R., Gelman, A., & Blei, D. M. 2016, arXiv:1603.00788
- Kunkel, W. E. 1970, *PASP*, **82**, 1341
- Kunkel, W. E. 1973, *ApJS*, **25**, 1
- Lightkurve Collaboration, Cardoso, J. V. D. M., Hedges, C., et al. 2018, *Lightkurve: Kepler and TESS Time Series Analysis in Python*, Astrophysics Source Code Library, ascl:1812.013
- Lomax, J. R., Wisniewski, J. P., Roberge, A., et al. 2018, *AJ*, **155**, 62
- Luger, R., Agol, E., Foreman-Mackey, D., et al. 2019, *AJ*, **157**, 64
- Macintosh, B., Graham, J. R., Barman, T., et al. 2015, *Sci*, **350**, 64
- Malo, L., Doyon, R., Feiden, G. A., et al. 2014, *ApJ*, **792**, 37
- Mamajek, E. E., & Bell, C. P. M. 2014, *MNRAS*, **445**, 2169
- Martoli, E., Hébrard, G., Correia, A. C. M., Laskar, J., & Lecavelier des Etangs, A. 2021, *A&A*, **649**, A177
- Montet, B. T., Bowler, B. P., Shkolnik, E. L., et al. 2015, *ApJL*, **813**, L11
- Nielsen, E. L., De Rosa, R. J., Wang, J., et al. 2016, *AJ*, **152**, 175
- Notsu, Y., Shibayama, T., Maehara, H., et al. 2013, *ApJ*, **771**, 127
- Perez, F., & Granger, B. E. 2007, *CSE*, **9**, 21
- Pitkin, M., Williams, D., Fletcher, L., & Grant, S. D. T. 2014, *MNRAS*, **445**, 2268
- Plavchan, P., Barclay, T., Gagné, J., et al. 2020, *Natur*, **582**, 497
- Ricker, G. R., Winn, J. N., Vanderspek, R., et al. 2015, *JATIS*, **1**, 014003
- Robertson, P., Stefansson, G., Mahadevan, S., et al. 2020, *ApJ*, **897**, 125
- Rodono, M., Cutispoto, G., Pazzani, V., et al. 1986, *A&A*, **165**, 135
- Salvatier, J., Wiecki, T. V., & Fonnesbeck, C. 2016, *PeerJ Comp. Sci.*, **2**, e55
- Shkolnik, E. L., Allers, K. N., Kraus, A. L., Liu, M. C., & Flagg, L. 2017, *AJ*, **154**, 69
- Smith, J. C., Stumpe, M. C., Van Cleve, J. E., et al. 2012, *PASP*, **124**, 1000
- Stauffer, J., Tanner, A. M., Bryden, G., et al. 2010, *PASP*, **122**, 885
- Stumpe, M. C., Smith, J. C., Catanzarite, J. H., et al. 2014, *PASP*, **126**, 100
- Stumpe, M. C., Smith, J. C., Van Cleve, J. E., et al. 2012, *PASP*, **124**, 985
- Theano Development Team 2016, arXiv:1605.02688
- Torres, C. A. O., Ferraz Mello, S., & Quast, G. R. 1972, *ApL*, **11**, 13
- Vanderspek, R., Doty, J. P., Fausnaugh, M., et al. 2018, *TESS Instrument Handbook v0.1*, Technical Report
- Wilson, O., & Woolley, R. 1970, *MNRAS*, **148**, 463
- Zuckerman, B., Song, I., Bessell, M. S., & Webb, R. A. 2001, *ApJL*, **562**, L87